Available online at www.sciencedirect.com

ScienceDirect

Geochimica et Cosmochimica Acta xxx (2018) xxx–xxx

Geochimica et Cosmochimica Acta

www.elsevier.com/locate/gca

Iodate in calcite, aragonite and vaterite $CaCO_3$: Insights from first-principles calculations and implications for the I/Ca geochemical proxy

Xiaolei Feng [a], Simon A.T. Redfern [a,b,*]

[a] Department of Earth Sciences, University of Cambridge, Downing Street, Cambridge CB2 3EQ, UK
[b] Center for High Pressure Science and Technology Advanced Research (HPSTAR), Shanghai 201203, China

Received 3 August 2017; accepted in revised form 6 February 2018; available online xxxx

Abstract

The incorporation of iodine into each of the three polymorphs of $CaCO_3$ – calcite, aragonite and vaterite, is compared using first-principles computational simulation. In each case iodine is most easily accommodated as iodate (IO_3^-) onto the carbonate site. Local strain fields around the iodate solute atom are revealed in the pair distribution functions for the relaxed structures, which indicate that aragonite displays the greatest degree of local structural distortion while vaterite is relatively unaffected. The energy penalty for iodate incorporation is least significant in vaterite, and greatest in aragonite, with the implication that iodine will display significant partitioning between calcium carbonate polymorphs in the order vaterite > calcite > aragonite. Furthermore, we find that trace iodine incorporation into vaterite confers improved mechanical strength to vaterite crystals. Our results support the supposition that iodine is incorporated as iodate within biogenic carbonates, important in the application of I/Ca data in palaeoproxy studies of ocean oxygenation. Our observation that iodate is most easily accommodated into vaterite implies that the presence of vaterite in any biocalcification process, be it as an end-product or a precursor, should be taken into account when applying the I/Ca geochemical proxy.

Keywords: Carbonate; Iodine; Iodate

1. INTRODUCTION

Understanding seawater oxygen content is important, since oxygen minimum zones (OMZs) adversely affect marine fisheries and biological productivity. Oxygen depletion appears to be affecting a greater and greater volume of intermediate ocean waters, and has been associated with ocean warming and climate change (Keeling et al., 2010). Understanding the climate sensitivity of the oceans' oxygen minimum zone, both today and over geological time scales, demands the development of a geochemical proxy for water oxygen content. As a redox-sensitive element, iodine has been proposed as a suitable proxy for this purpose. Iodine has been recognised as a promising geochemical indicator for oxygen content: the variation of speciation of iodine in seawater, as either iodide (I^-) or iodate (IO_3^-) anions, and the iodide/iodate redox potential lies close to that of O_2/H_2O (Rue et al., 1997). As oxygen content decreases, the speciation of iodine in aqueous solutions changes from dominantly iodate to iodide, and iodide is thermodynamically stable in anoxic waters (Chapman and Truesdale, 2011). Iodine accumulates in planktonic and benthic marine calcifiers, and follows a nutrient-like vertical distribution in the oceans (Elderfield and Truesdale, 1980). Diagenetic processes may act as a further control on the presence of iodine

* Corresponding author at: Department of Earth Sciences, University of Cambridge, Downing Street, Cambridge CB2 3EQ, UK.
E-mail address: satr@cam.ac.uk (S.A.T. Redfern).

https://doi.org/10.1016/j.gca.2018.02.017
0016-7037/

in pore fluids (Kennedy and Elderfield, 1987). Since I^- does not enter carbonate minerals, while IO_3^- does, the iodine content of marine carbonates may be used as a proxy for seawater [O_2]. More generally, halogens play an important part in Earth's ecosystems, and volcanic emissions of halogens are known to be considerable, but most studies to date have focussed on chlorine and fluorine. Typical concentrations of iodine in carbonate rocks lie in the ppm range (Fuge and Johnson, 1986) and may range as high as 500 nM in ocean waters (Hardisty et al., 2017). The fates of iodine in the solid Earth, in crustal and mantle rocks and reservoirs, and its sources, sinks and fluxes, remain undefined and largely unknown, although the possible transfer of iodine into the mantle through subducted oceanic sediments remains a clear possibility.

Inorganic precipitation experiments have found that I/Ca ratios in calcites crystallised from solution are linearly-dependent upon the IO_3^- concentration of the parent water, but are independent of I^- content of such water (Lu et al., 2010). Lu et al. (2010) carried out experiments in which they grew synthetic calcites spiked with iodine in solution, either as iodide or iodate. While they found little dependence of the I/Ca ratios in their samples for the iodide-bearing solutions, they saw a linear relationship between I/Ca and iodate concentration and concluded that the likely substitution mechanism is IO_3^- substituting for the CO_3^{2-} oxy-anion in calcite: since IO_3^- occurs in oxygenated water, the I/Ca ratio was found to be higher in the test of foraminifera grown in high [O_2] water. Their interest was in the application of measurements of iodine in calcite as a geochemical proxy for seawater redox potential, given the fact that iodate/iodide speciation changes with the oxidation state of seawater. This is particularly interesting because I/Ca in benthic foraminifera provide a route to measuring the variations in oxygen contents of bottom waters (Glock et al., 2014). Additionally, low I/Ca ratios in fossil planktonic foraminifera have been identified with ocean anoxia in the stagnant oceans of the mid-Cretaceous, associated also with organic-rich clay-bearing sediments (Zhou et al., 2015). In the same way that B, Mg and Na have been seen to vary through the test wall of a foraminifera (Branson et al., 2013; Branson et al., 2015; Redfern et al., 2017), so I/Ca ratios also display heterogeneity, in the basis of ICP-MS measurements (Glock et al., 2016). If such intra-test heterogeneities are indeed caused by variations in the redox-conditions over the lifetime of a single foraminiferal specimen, it may even be possible to reconstruct relative [O_2] changes in bottom waters on sub-annual time scales, although the biological controls on iodine incorporation are unclear. These previous studies made no direct measurement, by spectroscopy or other structural means, of the speciation and incorporation state of the iodine in their samples, however. A fully quantitative relationship between dissolved oxygen and foraminiferal I/Ca has yet to be developed, and inferences from I/Ca remain qualitative. None the less, the fate of iodine in biogenic carbonates has been found to be a reliable indicator of ocean oxidation state, with results from foraminiferal calcite being employed to infer bathymetric variations in deoxygenation of ancient and modern oceans (Zhou et al., 2014; Lu et al., 2016), for example.

It is worth noting that further interest in the fate of iodine in the near surface solid Earth and in ground waters has arisen due to its prevalence in nuclear waste materials. Iodine has one stable isotope, ^{127}I, but twenty-five radioactive isotopes and ^{131}I is an acute radioactive contaminant. Due to its long half-life (1.6×10^7 yrs), high inventories in typical spent fuel, high bioactivity and high mobility, ^{129}I released into the environment has been identified as a major potential hazard in groundwater near nuclear waste disposal sites (Gephart, 2010; Kaplan et al., 2011; Kaplan et al., 2014). Understanding the interaction between iodine in aqueous solution and carbonate mineral precipitates in sediments (as well as in concrete repository structures) is crucial in understanding the pathways and risks from ^{129}I. Much of the ^{127}I and ^{129}I that originally existed as aqueous species in contaminated groundwater at the Hanford nuclear site co-precipitated into groundwater calcite, mainly as iodate (Zhang et al., 2013), demonstrating the important role in the geochemical immobilization of radioactive iodine played by the interaction between $CaCO_3$ and aqueous iodine species.

In order to better understand the incorporation of iodine into carbonates, it is necessary to first determine the ultimate location of iodine within carbonate mineral structures. Several early studies tackled the incorporation of trace and major elements into calcite but they mainly focused on exchange of Ca^{2+} with other cations, such as Mg^{2+}, Na^+, Fe^{2+}, Zn^{2+}, As^{5+}, Sr^{2+}. More recently, attention has turned to anion substitutions into carbonates, building on earlier work characterizing sulfate incorporation into carbonate minerals (Takano et al., 1980). Electron paramagnetic resonance (EPR) spectroscopy and X-ray diffraction have been used to study the possible incorporation of SO_4^{2-}, NO_3^- and Cl^- into the calcite crystal structure and to find out the possible sites and mode of their incorporation (Kontrec et al., 2004). The results indicated that the calcite lattice becomes distorted due to the incorporation of such anions. Based on these studies, it was concluded that sulfate can be incorporated into the calcite lattice and substitute for carbonate ions. Their results were supported by a number of later experimental investigations (Takano et al., 1980; Fernández-Díaz et al., 2010; Balan et al., 2017). Extended X-ray absorption fluorescence spectroscopy (EXAFS) was also used to determine how the tetrahedral SeO_4^{2-} species are accommodated in the bulk calcite structure (Reeder et al., 1994; Lamble et al., 1995). Lamble et al. (1995) found that tetrahedral SeO_4^{2-} oxy-anions substitute for trigonal CO_3^{2-} in calcite. As far as iodine incorporation is concerned, an X-ray single crystal electron density study of calcite Maslen et al. (1993) attempted to infer the influence of dilute iodate incorporation and postulated that it substitutes for the carbonate ion in calcite based on the fact that the Ca–O distance in calcium iodate, $Ca(IO_3)_2$, is similar to that in calcite. Most recently, Podder et al. (2017) used a combination of X-ray absorption spectroscopy and first principles calculations to identify the nature of iodate in calcite and vaterite, confirming that this is the dominant incorporation mode.

Here, we extend our understanding of the incorporation of iodine in calcium carbonates using *ab initio* computa-

Please cite this article in press as: Feng X. and Redfern S. A. T. Iodate in calcite, aragonite and vaterite $CaCO_3$: Insights from first-principles calculations and implications for the I/Ca geochemical proxy. *Geochim. Cosmochim. Acta* (2018), https://doi.org/10.1016/j.gca.2018.02.017

tional simulations of iodine substitution for carbon in the carbonate group as well as for Ca at the large cation site, within all three ambient pressure/temperature polymorphs of calcium carbonate, namely calcite, aragonite and vaterite, with the aim of quantifying the local distortion effects and estimating the likely enthalpic penalties of iodine incorporation. Early simulation studies of carbonates, and calcite in particular, adopted atomistic models to understand trace element substitutions (e.g. Archer et al., 2003), but more recently *ab initio* methods such as density functional theory have been adopted successfully to understand the effects locally of trace or minor anionic element substitutions, including those of sulphate, selenite, and bromate oxy-anions within carbonate (Balan et al., 2014, 2016, 2017; Arroyo-de Dompablo et al., 2015).

2. METHODS

The energetics and physical properties of three polymorphs of calcium carbonate, $CaCO_3$, namely calcite, aragonite and vaterite, were calculated using first-principles structure methods based on density functional theory. Calculations were performed employing the Vienna *ab initio* simulation package (Kresse and Furthmüller, 1996). The generalized gradient approximation (Perdew et al., 1992) in the scheme of the Perdew–Burke-Enzerhoff (Perdew et al., 1996) pseudopotentials was used, alongside projected-augmented-wave (PAW) potentials (Perdew et al., 1992; Perdew et al., 1996) for electron–ion interactions. PAW potentials with $3s^2 3p^4 4s^2$, $2s^2 2p^2$, $2s^2 2p^4$, and $5s^2 5p^5$ electrons as valence electrons were adopted for the Ca, C, O and I atoms respectively. A kinetic energy cutoff of 500 eV was chosen, and Monkhorst-Pack meshes for Brillouin zone sampling were selected with a resolution of 0.3 $Å^{-1}$. Elastic constants were computed from the strain-stress method, and the bulk modulus, shear modulus, Young's modulus and Poisson's ratio were derived from the Voigt-Reuss-Hill averaging scheme (Hill, 1952).

The incorporation of iodine into pure calcium carbonate was treated as an impurity substitutional defect. Two different basic approaches can usually be used to model an impurity in a crystal. In the first, the full system geometry is relaxed at zero pressure. This approach accounts for the variation of cell parameters observed for relatively high impurity concentrations (i.e. partial solid solutions). However, because of periodic boundary conditions, only an ordered distribution of impurities in the crystal is actually considered and this may artificially affect the symmetry of the whole. Alternatively, a relaxation of the impurity-bearing model can be performed with the volume of the pure crystal maintained, which makes the simplifying assumption the symmetry and molar volume of the bulk crystal should not be affected by the presence of an impurity at low concentration. In this case, computational limits prevent calculation of very large super-cells and a stress is usually observed over the super-cell, due to residual elastic interactions between the impurity and its periodic images. We have adopted both approaches to make a comparison of the enthalpies determined from each of the methods. The starting structure for the computational work on calcite, aragonite and vaterite was that of *R*-3*c*, *Pnma*, and *Cc* respectively. The structures of *R*-3*c* calcite and *Pnma* aragonite are well-known and among the first to be identified in the early history of crystallographic studies. We used the structures of Graf (1961) and De Villiers (1971) as starting points for our calculations. The structure of vaterite is much-debated, however, and we therefore did not use any of the experimentally-derived structures. We choose, instead, the theoretically calculated *Cc* structure, containing 12 formula units of $CaCO_3$ per unit cell (Demichelis et al., 2013b) for the convenience of making a supercell containing the same number of atoms for all three polymorphs (detailed structural information is given in Table S2 in the supporting information). A super-cell containing 24 formula units of $CaCO_3$ (120 atoms) was constructed for each of the polymorphs. In the case of calcite, a supercell was chosen that corresponds to four conventional hexagonal unit cells. The supercell was, therefore, constructed as $2a \times 2b \times c$ where *a, b*, and *c* are the cell parameters of the hexagonal setting of the calcite *R*-3*c* unit cell. For aragonite, the simulation cell comprised six times the volume of the conventional unit cell, with a supercell constructed as $2a \times 3b \times c$, where *a, b*, and *c* are the cell parameters of the orthorhombic *Pnma* unit cell of aragonite. For vaterite, the simulation cell comprised twice the volume of the conventional unit cell, with a supercell constructed as $a \times 2b \times c$, where *a, b*, and *c* are the cell parameters of the monoclinic *Cc* unit cell of vaterite. The structures were relaxed, with atomic relaxation terminated when the change in the total energy per atom converged within 1 meV.

3. RESULTS

The enthalpy (we list the enthalpies of all the structures considered in this work in Table S1 in the supporting information) of pure calcite was found to be lower than that of the aragonite and vaterite. It should be noted, however, that the differences in enthalpies of these three polymorphs of $CaCO_3$ are generally similar to the distribution of estimates of enthalpy that are provided by different density functionals (Demichelis et al., 2013a) and that calcite is stabilized against the other polymorphs at ambient by entropic effects, especially associated with carbonate rotational disorder at high temperatures (Redfern et al., 1989). In order to evaluate the reliability of our simulations further, experimental values of lattice parameters for carbonates (calcite and aragonite) are also given in Table 1 and show good structural correspondence. The GGA functional, the most commonly used for solids, is well known to overestimate the lattice constants with typical errors amounting up to 2% (He et al., 2014). Here, the lattice constants of our simulation are larger than that of experimental values by 0.8–1.7%. Our simulations are, therefore, in reasonably good agreement with experiment.

Using the relaxed structures as a starting point for the next stage of the calculations, the properties of iodine-doped equivalents were calculated by introducing one iodine atom into each of the supercells in two substitution

Please cite this article in press as: Feng X. and Redfern S. A. T. Iodate in calcite, aragonite and vaterite $CaCO_3$: Insights from first-principles calculations and implications for the I/Ca geochemical proxy. *Geochim. Cosmochim. Acta* (2018), https://doi.org/10.1016/j.gca.2018.02.017

Table 1
Comparison of structural information (including space group, lattice parameters and Wyckoff positions) for carbonates and iodine-bearing carbonates, including both calcite and aragonite (available experimental values are also listed).

Phase	Structure	Space group	Volume (Å^3)	Lattice parameter
Calcite	Experimental[a]	*R*3*c*	367.9	$a = b = 4.99$ Å; $c = 17.06$ Å $\alpha = \gamma = 90.0°$; $\beta = 120°$
	Unit cell	*R*3*c*	381.5	$a = b = 5.05$ Å; $c = 17.26$ Å $\alpha = \gamma = 90.0°$; $\beta = 120°$
	Supercell	*R*3*c*	1526.0	$2a = 2b = 10.11$ Å; $c = 17.26$ Å $\alpha = \gamma = 90.0°$; $\beta = 120°$
	Iodine-bearing	$P32_1$	1541.9	$a = b = 10.17$ Å; $c = 17.22$ Å $\alpha = \gamma = 90.0°$; $\beta = 120°$
Aragonite	Experimental[b]	*Pnma*	226.9	$a = 5.704$ Å; $b = 4.961$ Å; $c = 7.967$ Å $\alpha = \beta = \gamma = 90.0°$
	Unit cell	*Pnma*	233.5	$a = 5.803$ Å; $b = 5.011$ Å; $c = 8.031$ Å $\alpha = \beta = \gamma = 90.0°$
	Supercell	*Pnma*	1401.1	$2a = 11.606$ Å; $3b = 15.032$ Å; $c = 8.031$ Å $\alpha = \beta = \gamma = 90.0°$
	Iodine-bearing	*Pm*	1435.0	$a = 11.735$ Å; $b = 15.253$ Å; $c = 8.017$ Å $\alpha = \gamma = 90.0°$; $\beta = 89.847°$
Vaterite	Demichelis[c]	*Cc*		$a = 12.281$ Å; $b = 7.142$ Å; $c = 9.371$ Å $\alpha = \gamma = 90.0°$; $\beta = 115.5°$
	Unit cell	*Cc*	782.4	$a = 12.561$ Å; $b = 7.300$ Å; $c = 9.457$ Å $\alpha = \gamma = 90.0°$; $\beta = 115.6°$
	Supercell	*Cc*	1564.7	$a = 12.561$ Å; $b = 14.600$ Å; $c = 9.457$ Å
	Iodine-bearing	*P*2	1577.5	$a = 12.617$ Å; $b = 14.550$ Å; $c = 9.527$ Å $\alpha = \gamma = 90.0°$; $\beta = 115.7°$

[a] Experimental values from Graf (1961).
[b] Experimental values from De Villiers (1971).
[c] Theoretical values from Demichelis et al. (2013a, 2013b).

mechanisms. One involved the substitution of iodine for calcium, onto the large octahedral site. The other corresponded to the substitution of iodine for carbon, as an iodate replacing the carbonate group. In each case the modified structures correspond to an average site occupancy of around 4% substitution of iodine onto the site. Our calculations do not assume the oxidation state of iodine, but simply find the lowest enthalpy configuration based on the pseudo-potential model. We adopted two approaches. In the first, the iodine-substituted structures were constructed without imposing any symmetry restrictions (by starting from a set of atomic positions equivalent to the host phase but with the symmetry then reduced to *P*1) and then optimized under no symmetry restrictions. The symmetries of the resultant structures were then analysed and it was found that they were $P32_1$ for iodine-substituted calcite, *Pm* for the iodine-substituted aragonite structure and *P*2 for iodine-substituted vaterite. It should be stressed that we are not suggesting that iodine substitution at the ppm level, as seen in nature, would result in reduction of the long-range space group symmetry of a carbonate host crystal to these symmetries. Rather, these represent the symmetry of the local distortion that is to be expected around an iodine substituent atom when hosted within such a phase.

An alternative approach was then adopted (to compare with the structurally-unconstrained approach), in which the density of the host carbonate structure was maintained by fixing the unit cell parameters, and a single iodine atom substituted into the structure with the metric unit cell of the host lattice maintained, without any further relaxation of the volume or unit cell parameters.

When performing the substitution, every possible atomic replacement needs to be taken into consideration. Since all the carbon atoms are symmetrically equivalent in calcite and aragonite, there is only one way to do the C-site substitution. This is also true for the Ca-site substitution. In vaterite, however, there are three symmetrically distinct carbon atoms in a unit cell, and there are therefore three ways to replace one carbon atom with one iodine atom. We accordingly tried all the three possible substitutions and discuss only the one with lowest energy henceforth (see Table S1 in the supplementary information). It is worth noting that the space group of the vaterite iodine-substituted structure with lowest energy is *P*2, while the symmetry of the other two reduced to *P*1. There are also three possible Ca-site substitutions in vaterite, with the most stable one having $P-1$ after iodine substitution, and the other two less-favoured structures having *P*1 symmetry.

Please cite this article in press as: Feng X. and Redfern S. A. T. Iodate in calcite, aragonite and vaterite $CaCO_3$: Insights from first-principles calculations and implications for the I/Ca geochemical proxy. *Geochim. Cosmochim. Acta* (2018), https://doi.org/10.1016/j.gca.2018.02.017

4. DISCUSSION

From the results of the calculations of enthalpies for each of the relaxed structures, combined with the enthalpies for elemental Ca, C, and I under the same conditions, we have determined the enthalpies associated with substitutional iodine incorporation via the following reactions for all the three polymorphs of $CaCO_3$:

$$24(Ca(CO_3)) + 0.5I_2 \Rightarrow Ca_{23}I(CO_3)_{24} + Ca \quad (1)$$

$$24(Ca(CO_3)) + 0.5I_2 \Rightarrow Ca_{24}(CO_3)_{23}(IO_3) + C \quad (2)$$

Calculated enthalpies for each of the reactants and products (see Table S1 in the supplementary information) allow us to determine the enthalpies of reaction for each of the $CaCO_3$ polymorphs. It is worth noting that incorporation of iodine in calcium carbonates is expected to result in some charge deficit that must be compensated, and this can be accounted for using either a homogeneous electrostatic background or a coupled heterovalent substitution. We have used the first of these methods to maintain the electric neutrality of the system, but charge compensation mechanisms in natural iodine-bearing carbonates may play an important role. Iodine itself can adopt multiple valence states, with I^{3+} and I^{5+} each forming iodite or iodate oxyanions in nature. In view of this it is quite possible that iodine incorporation and substitution for C^{4+} in the carbonates that we have considered is accommodated by variable oxidation state of the iodine itself. Alternatively, coupled substitution of Ca^{2+} at the large octahedral M-site, for example by monovalent Na^+ might reasonably occur, via a mechanism such as $Na^+ + I^{5+} \Leftrightarrow Ca^{2+} + C^{4+}$. Indeed, this mechanism has been considered previously, for carbonates, and shown to be effective (Podder et al., 2017). In this case, the incorporation of iodine may enhance the propensity for incorporation of sodium, and vice versa. We are not aware of any studies of the correlation between I/Ca values and other proxy measures, such as Na/Ca, but conducting such combined measurements offers a route to understanding the influence of individual trace elements on the concentrations of others. The detail of the possible coupled substitutions are undoubtedly likely to be influenced by vital processes within the calcifying space of a biomineralising organism. Other monovalent alkali ions could just as well take part in the coupled substitution of $M^+ + I^{5+} \Leftrightarrow Ca^{2+} + C^{4+}$, where M = Li, Na, K, Rb or Cs, for example. It would be instructive to explore correlations between iodine concentrations and the concentrations of any of these alkali ions.

We find that the energies of the iodine-bearing structures that we obtain from either method of structural relaxation (maintaining the metric unit cell of the host or allowing the structure to completely relax) are essentially identical within the accuracy of the calculations (Table S1). Furthermore, we have calculated the enthalpies using an alternative cross-correlation functional within the local density approximation (LDA) to check that the choice of functional (GDA[PBE] vs LDA) does not affect our conclusions. From the results shown in Table S1 it is clear that the choice of functional does affect the absolute values of enthalpy for the three phases, but does not change the relative sizes of the enthalpies and thus does not alter our conclusions. Hereafter, therefore, we restrict our discussion to the results pertaining to the GDA[PBE]-derived structures, in which full structural relaxation was allowed under no symmetry or metric cell constraints. These structures most accurately represent the "local distorted symmetry" corresponding locally to the iodine environment.

The energies of the two substitution reactions (Ca-site and C-site substitution) for calcite are +40.5 and +25.7 kJ/mol respectively. Equivalent values for substitutions into the aragonite form of $CaCO_3$ are +38.7 and +30.3 kJ/mol. Finally, equivalent values for substitutions into the vaterite form of $CaCO_3$ are +34.2 and +22.5 kJ/mol. It is worth noting that our calculations correspond to zero pressure and zero temperature (0 K) conditions. In the absence of any other factors, the bare thermodynamic influence of increased temperature might be expected to favour iodate incorporation due to the entropic advantage, in the same way that the Mg/Ca geochemical proxy for temperature works (Elderfield and Ganssen, 2000). However, preliminary results on synthetic iodine-bearing calcites (Zhou et al., 2014) suggested lower partition coefficients for iodate at higher temperatures. Establishing the origin of this observed temperature-dependence of iodine partitioning is beyond the scope of our work, which offers little insight into the potential mechanisms. One might speculate, however, that the experimentally-observed reduction in iodate partitioning into calcite with temperature could be related to the temperature-dependence of iodine speciation in aqueous solutions, as controlled by iodine hydrolysis (Burns et al., 1990). Further complicating factors could include kinetic effects associated with dissolution/re-precipitation reactions of the carbonate itself.

Our results demonstrate unequivocally that iodate substitution into calcite involves a lower energy penalty than substitution into aragonite, and that iodine is expected, therefore, to partition as iodate into calcite over aragonite. However, substitution into vaterite appears even more favourable than into either of the two other phases. Thus, although vaterite is metastable with respect to calcite as pure $CaCO_3$, incorporation of iodine as a defect substitution is less prohibitive into the vaterite structure than into either aragonite or calcite. This demonstrates that vaterite has greater capacity for incorporation of minor impurities in solid solution. Furthermore, our results indicate that iodine favours incorporation onto the C-site over the Ca-site in all three polymorphs, that is to say, iodine substitution as IO_3^-, replacing the CO_3^{2-} carbonate group, is by far the most favourable substitutional reaction. We therefore focus our analyses on this C-site incorporation.

To understand the energy difference, it is first necessary to look at the effect each iodine substitution has upon the crystal lattice. Structural details of iodine-bearing carbonates, including calcite, aragonite and vaterite, are listed in Table 1 along with those of pure carbonate structures (a table with more detailed structural information – including atomic coordinates – is given in the supplementary information as Table S2, and CIF data are available online at doi: http://doi.org/10.17632/vvypr24z7k.2). The substitution of IO_3^- for the CO_3^{2-} carbonate group results in a local modi-

Please cite this article in press as: Feng X. and Redfern S. A. T. Iodate in calcite, aragonite and vaterite $CaCO_3$: Insights from first-principles calculations and implications for the I/Ca geochemical proxy. *Geochim. Cosmochim. Acta* (2018), https://doi.org/10.1016/j.gca.2018.02.017

fication of the structure, with local distortions and with a significant change of lattice parameters. In particular, the incorporation of the larger iodine atom (compared with carbon atom) induces obvious local distortion around the hosted iodine atom in the calcium carbonate structures, including calcite, aragonite and vaterite, as seen in Fig. 1.

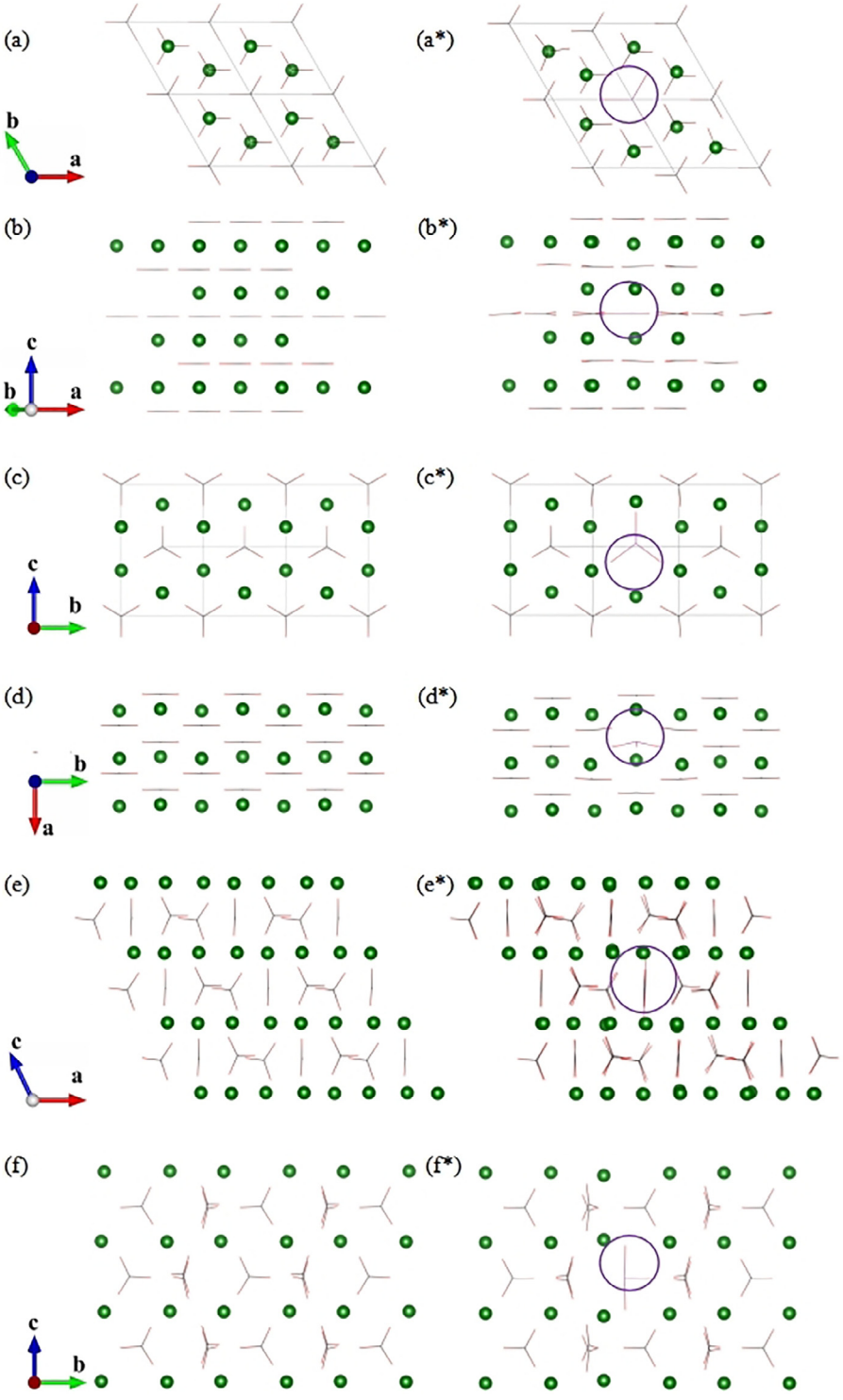

Fig. 1. Distortion due to the iodine substitution for carbon atoms in calcite (a, a*, b, b*), aragonite (c, c*, d, d*) and vaterite (e, e*, f, f*), showing the asymmetrical distortion in aragonite and vaterite compared to the higher symmetry centrosymmetric distortion of the calcite structure. Ca, Ca, O and I atoms are shown in green, black, red and purple, respectively. (For interpretation of the references to color in this figure legend, the reader is referred to the web version of this article.)

Please cite this article in press as: Feng X. and Redfern S. A. T. Iodate in calcite, aragonite and vaterite $CaCO_3$: Insights from first-principles calculations and implications for the I/Ca geochemical proxy. *Geochim. Cosmochim. Acta* (2018), https://doi.org/10.1016/j.gca.2018.02.017

For calcite, the lattice of the iodine-bearing structure remains rhombohedral, even in the immediate vicinity of the iodine substituent, although (locally) the space group symmetry is lowered from $R3c$ in pure calcite to $P32_1$ in the vicinity of the defect in iodine-bearing calcite. Iodine sits in planar triangular coordination, with the same coordination geometry as carbon in CO_3, but he introduction of IO_3 groups causes out-of-plane tilts of both the IO_3 and CO_3 molecules within the layers lying parallel to the hexagonal (0 0 1) planes. For comparison, the unit cell parameters of the supercell of calcite (with volume and number of atoms similar to its iodine-bearing counterpart) are also given in Table 1. As can be seen from this table, in order to accommodate the iodine atom, whose atomic radius is twice that of the carbon atom, the volume of the unit cell increases by lengthening along both the a and b axes, which define the layers parallel to the (0 0 1) plane on which the carbonate groups lie.

In iodine-bearing aragonite, the original orthorhombic cell reduces in symmetry to monoclinic after substitution of one in 24 carbon atoms by iodine and relaxation of the unit cell. This is revealed as a very subtle change of the β, angle from 90° to 89.847° (a shear strain of 2.7×10^{-3}) and results in a local symmetry for the iodine-bearing aragonite of Pm. The incorporation of iodine atoms enlarges the aragonite unit cell locally, in the same way as is seen in calcite, principally as a significant increase of the b cell parameter, along which direction the carbonate/iodate groups are aligned in rows. It is worth noting that, unlike the case of calcite or vaterite, the coordination of iodine by oxygen is irregular trigonal pyramidal, which is similar to the iodate coordination geometry in calcium iodate, although the coordination is distorted and much closer to triangular planar than that of iodate in calcium iodate. The iodate molecule in iodine-bearing aragonite shows two O—I—O bond angles of 123.6° and one of 103.7°, so all are relatively close to the triangular planar bond angle of 120°. In calcium iodate the equivalent bond angles are 98.7°, 98.7° and 98.3° and the iodate geometry is much more pyramidal (Peter et al., 1998). The oxygen atoms' out of plane movements relative to the aragonite-hosted iodine create local dipoles and the structure becomes locally-polar. This is interesting since the same phenomenon was reported in an early work which focused on substitutions onto the cation (Ca^{2+}) positions in these carbonates (Archer et al., 2003). It seems likely that the incorporation into aragonite, unlike other forms of carbonates, results in the formation of dipoles for a wider range of elemental substitutions.

In iodine-bearing vaterite, the phase which displays the smallest energy penalty for iodine incorporation, the symmetry of the host monoclinic structure is reduced around the iodate oxy-anion, resulting in a local $P2$ symmetry. The incorporation of iodine atom causes a small increase in the vaterite unit cell volume locally. There is subtle disruption of the orientations of the carbonate anions around the iodine atom, but the changes are not as obvious as for the other two polymorphs of $CaCO_3$ because the vaterite structure is already relatively disordered, with a wider range of CO_3 group orientations. Previous work on the substitute of sulfate into vaterite (Balan et al., 2014) found that the carbonate groups were less disrupted by the substitution (than for sulfate substitution in calcite or aragonite) but that the sulfate group itself was more distorted than when substituted into calcite or aragonite. We find precisely the same situation for iodine incorporation into vaterite, in comparison with calcite and aragonite, with the iodate group being highly distorted with two I—O bond of 1.975 Å and one of 1.874 Å, and two I—O—I bond angles of 88° and one of 176°.

The effects of iodate replacement for the carbonate ion are readily quantified by inspection and comparison of the radial distribution functions for the pure and iodine-bearing versions of these three polymorphs. The radial dis-

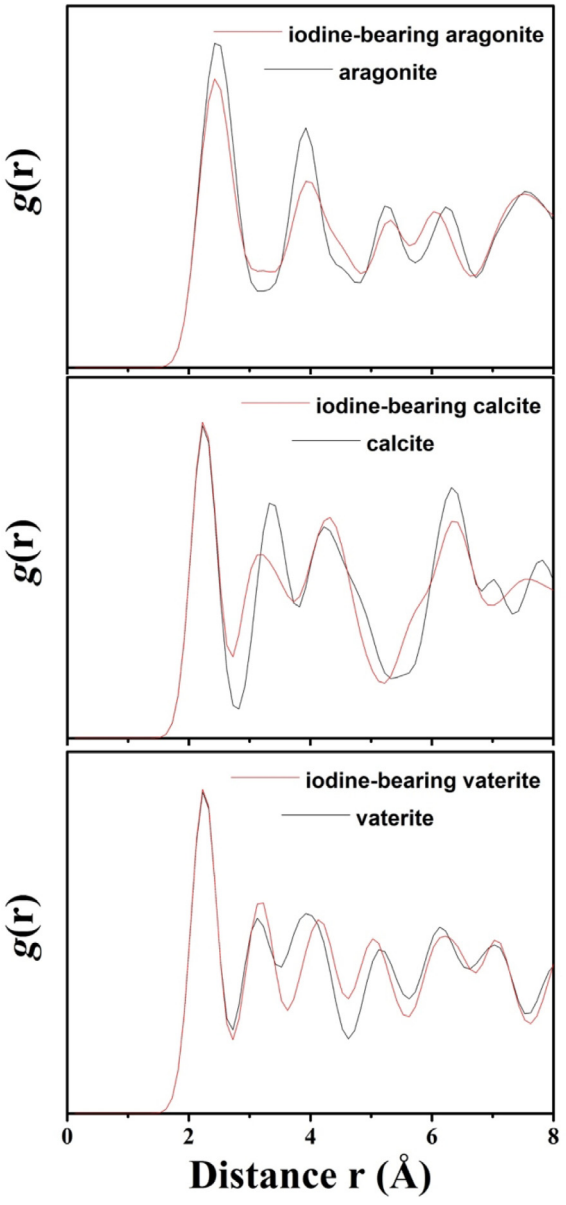

Fig. 2. Radial distribution functions (RDF) of carbonate and iodine-bearing carbonate, including calcite, aragonite and vaterite, with the calcium atom closest to the iodine atom at the origin.

Please cite this article in press as: Feng X. and Redfern S. A. T. Iodate in calcite, aragonite and vaterite $CaCO_3$: Insights from first-principles calculations and implications for the I/Ca geochemical proxy. *Geochim. Cosmochim. Acta* (2018), https://doi.org/10.1016/j.gca.2018.02.017

tribution functions for these six structures (iodine-free and iodine-bearing calcite, aragonite and vaterite) are shown, plotted as $g(r)$, in Fig. 2, where the distribution of electron density away from a central calcium atom (closest to iodine) is plotted. In aragonite, the first shell of atoms away from calcium is affected by the incorporation of iodine with a noticeable change in the height of this first shell peak for the iodine-aragonite. In comparison, the calcite and vaterite first shell peak is hardly changed by the incorporation of iodine. This likely accounts for the larger energy cost for iodine incorporation into aragonite compared to into calcite or vaterite. Comparing these latter two polymorphs, we see that the longer-range structure of iodine-bearing and iodine-free vaterite are rather similar to each other, while the same range of structure in calcite shows more significant perturbation upon iodine incorporation. Indeed, it is apparent that iodine may be accommodated into the vaterite structure with rather a small structural distortion penalty.

Finally, we have computed some of the physical properties of the structures that we have predicted. The elastic constants and mechanical properties of each of the three polymorphs, including their iodine-bearing equivalents, are presented in Table 2. Experimental measurements of the elastic properties of vaterite have not been carried out due to the difficulty in performing such measurement on this highly metastable phase, so we have compared our results with the computational results of Demichelis et al. (2013b). The calculated elastic constants of the iodine-free $CaCO_3$ polymorphs agree well with experimental observations, providing further confidence in our results for the iodate-bearing versions of each phase. The incorporation of iodine acts to slightly soften the structures of calcite and aragonite, but has the opposite effect in the vaterite structure. The consequence is that the iodine-bearing vaterite is stiffer than iodine-bearing aragonite, as well as pure $CaCO_3$ vaterite, further underlining the important nature of this phase in the potential incorporation of iodine in natural systems. Furthermore, we have found that iodine incorporation into calcium carbonate is energetically favoured in vaterite, compared with calcite or aragonite (the least favoured). The sequence vaterite > calcite > aragonite for ease of iodate incorporation is identical to that found for sulfate incorporation previously (Balan et al., 2014). Additionally, we find that iodine incorporation into vaterite lends this carbonate improved mechanical properties. This may be important in biomineralogical "deployment" of vaterite in organisms. It has been observed, for many organisms, that vaterite mineralization occurs when organisms suffer unfavourable stress conditions, such as disease or degraded environmental drivers (Frenzel and Harper, 2011). If such vaterite is also more able to accommodate trace elements, and by doing so able to develop improved strength and mechanical properties, such improvements may help explain the occurrence of vaterite in these organisms under these circumstances.

It is interesting to note that, as well as our predicted higher I/Ca ratio for vaterite over calcite or aragonite, Mg/Ca and Mn/Ca ratios are also observed to be higher in vaterite (in eel otoliths, as well as other biogenic vaterites) than in aragonite (Tzeng et al., 2007). Similar variations in geochemical proxy amplitudes between vaterite and aragonite or calcite have been seen in the calcified parts of a number of organisms including bivalves (Nehrke et al., 2012). As well as the implications that such variability has for the

Table 2
The calculated elastic constants C_{ij}, bulk modulus B, shear modulus G, Young's modulus Y_m (GPa) and Poisson's ratio P_r for pure carbonates (calcite, aragonite and vaterite) and iodine-bearing carbonates.

	Calcite				Aragonite			Vaterite	
	Exp[a]	Exp[b]	This work	Iodine-bearing	Exp[c]	This work	Iodine-bearing	This work	Iodine-bearing
C_{11}	149.4(7)	145.7	146.6	136.1	171.1(10)	167.3	96.1	80.7	86.6
C_{22}					110.1(9)	105.6	136.7	78.7	81.6
C_{33}	85.2(18)	85.3	87.6	83.7	98.4(12)	101.5	84.3	141.8	139.1
C_{44}	34.1(5)	33.4	32.6	30.4	39.3(6)	38.6	25.0	25.6	20.9
C_{55}	85.2(18)	85.3	87.6	83.7	98.4(12)	101.5	84.3	141.8	139.1
C_{66}	34.1(5)	33.4	32.6	30.4	39.3(6)	38.6	25.0	25.6	20.9
C_{12}	85.2(18)	85.3	87.6	83.7	98.4(12)	101.5	84.3	141.8	139.1
C_{13}	34.1(5)	33.4	32.6	30.4	39.3(6)	38.6	25.0	25.6	20.9
C_{14}	−20.0(2)	−20.5	17.8	14.5					
C_{15}							−0.7	−5.1	−4.0
C_{23}					41.9(20)	42.4	64.3	52.1	54.5
C_{24}							−5.6	−3.8	−3.6
C_{35}							3.4	−4.3	−2.8
C_{46}							−1.1	1.1	0.7
B			76.6	73.5	68.9(14)	69.0	62.2	61.4	65.1
G			32.2	29.2	35.8(2)	33.2	24.5	26.4	24.5
Y_m			84.6	77.4		85.9	65.2	69.3	65.2
P_r			0.316	0.324		0.292	0.331	0.312	0.333

[a] Experimental values from Chen et al. (2001).
[b] Experimental values from Dandekar and Ruoff (1968).
[c] Experimental values from Liu et al. (2005).

Please cite this article in press as: Feng X. and Redfern S. A. T. Iodate in calcite, aragonite and vaterite $CaCO_3$: Insights from first-principles calculations and implications for the I/Ca geochemical proxy. *Geochim. Cosmochim. Acta* (2018), https://doi.org/10.1016/j.gca.2018.02.017

importance of identifying the mineralogy of any calcium carbonate used for I/Ca geochemical proxy work, the potential enhancement of I/Ca in vaterite may also be important in understanding the origins of inherited iodine signatures. For example, it has recently been observed that foraminiferal calcite appears to be derived, in the early stages of calcification, from precursor vaterite (Jacob et al., 2017). In such circumstances, it is reasonable to conclude that the signatures measured in the stable "daughter" calcite phase of the test may well reflect the partitioning, under biological calcification, pertaining to the parent vaterite crystals.

5. CONCLUSIONS

The incorporation of iodine into all three naturally-occurring polymorphs of calcium carbonate – calcite, aragonite and vaterite, has been investigated via first-principles computational methods. In each case the incorporation of an iodine atom is favoured most strongly as substituent for carbon in the form of iodate, which causes local distortions of the structure over a length scale of around 10 Å. The local strain field around the iodate appears more extensive in aragonite than in the other two polymorphs, and the incorporation of iodine occurs with the least energy disadvantage into the vaterite structure. Furthermore, iodine-bearing vaterite shows improved mechanical strength compared to pure $CaCO_3$ vaterite. Our results confirm the expectation that iodine is incorporated as iodate within biogenic carbonates, and thus confirms the empirical observation that I/Ca may be employed as a proxy sensor representing the oxidation state of the water bodies within which such carbonates form. Furthermore, our observation that iodate is likely preferentially incorporated into the three polymorphs in order of ease vaterite > calcite > aragonite implies that the presence of vaterite in any biocalcification process, be it as an end-product or a precursor, needs to be taken into account when robustly applying the I/Ca geochemical proxy.

DATA

The structural (CIF) data and electron localisation functions for each calculated phase, that support the findings of this study, are available in Mendeley at doi: http://doi.org/10.17632/vvypr24z7k.2 accessible at http://doi.org/10.17632/vvypr24z7k.2.

ACKNOWLEDGEMENT

SATR acknowledges the support of NERC, grant NE/P019714/1 and XF is grateful for the support of the China Scholarship Council. The authors are grateful for many fruitful discussions over coffee with H. Elderfield, who stimulated this research and illuminated our understanding of trace element proxies in biogenic carbonates.

APPENDIX A. SUPPLEMENTARY MATERIAL

Supplementary data associated with this article can be found, in the online version, at https://doi.org/10.1016/j.gca.2018.02.017.

REFERENCES

Archer T. D., Birse S. E. A., Dove M. T., Redfern S. A. T., Gale J. D. and Cygan R. T. (2003) An interatomic potential model for carbonates allowing for polarization effects. *Phys. Chem. Miner.* **30**, 416–424.

Arroyo-de Dompablo M. E., Fernández-González M. A. and Fernández-Díaz L. (2015) Computational investigation of the influence of tetrahedral oxoanions (sulphate, selenate and chromate) on the stability of calcium carbonate polymorphs. *RSC Adv.* **5**, 59845–59852.

Balan E., Aufort J., Pouillé S., Dabos M., Blanchard M., Lazzeri M., Rollion-Bard C. and Blamart D. (2017) Infrared spectroscopic study of sulfate-bearing calcite from deep-seabamboo coral. *Eur. J. Mineral.* **29**, 397–408.

Balan E., Blanchard M., Pinilla C. and Lazzeri M. (2014) First-principles modeling of sulfate incorporation and 34S/32S isotopic fractionation in different calcium carbonates. *Chem. Geol.* **374–375**, 84–91.

Balan E., Pietrucci F., Gervais C., Blanchard M., Schott J. and Gaillardet J. (2016) First-principles study of boron speciation in calcite and aragonite. *Geochim. Cosmochim. Acta* **193**, 119–131.

Branson O., Kaczmarek K., Redfern S. A. T., Misra S., Langer G., Tyliszczak T., Bijma J. and Elderfield H. (2015) The coordination and distribution of B in foraminiferal calcite. *Earth Planet. Sci. Lett.* **416**, 67–72.

Branson O., Redfern S. A. T., Tyliszczak T., Sadekov A., Langer G., Kimoto K. and Elderfield H. (2013) The coordination of Mg in foraminiferal calcite. *Earth Planet. Sci. Lett.* **383**, 134–141.

Burns W. G., Matsuda M. and Sims H. E. (1990) Temperature dependence of the equilibrium constant for iodine hydrolysis at temperatures between 25 and 120° C. *J. Chem. Soc. Faraday Trans.* **86**, 1443–1447.

Chapman P. and Truesdale V. W. (2011) Preliminary evidence for iodate reduction in bottom waters of the Gulf of Mexico during an hypoxic event. *Aquat. Geochemistry* **17**, 671–695.

Chen C. C., Lin C. C., Liu L. G., Sinogeikin S. V. and Bass J. D. (2001) Elasticity of single-crystal calcite and rhodochrosite by Brillouin spectroscopy. *Am. Mineral.* **86**, 1525–1529.

Dandekar D. P. and Ruoff A. L. (1968) Temperature dependence of the elastic constants of calcite between 160 and 300 K. *J. Appl. Phys.* **39**, 6004–6009.

Demichelis R., Raiteri P., Gale J. D. and Dovesi R. (2013a) Examining the accuracy of density functional theory for predicting the thermodynamics of water incorporation into minerals: the hydrates of calcium carbonate. *J. Phys. Chem. C* **117**, 17814–17823.

Demichelis R., Raiteri P., Gale J. D. and Dovesi R. (2013b) The multiple structures of vaterite. *Cryst. Growth Des.* **13**, 2247–2251.

Elderfield H. and Ganssen G. (2000) Past temperature and δ18O of surface ocean waters inferred from foraminiferal Mg/Ca ratios. *Nature* **405**, 442–445.

Elderfield H. and Truesdale V. W. (1980) On the biophilic nature of iodine in seawater. *Earth Planet. Sci. Lett.* **50**, 105–114.

Fernández-Díaz L., Fernández-González Á. and Prieto M. (2010) The role of sulfate groups in controlling $CaCO_3$ polymorphism. *Geochim. Cosmochim. Acta* **74**, 6064–6076.

Frenzel M. and Harper E. M. (2011) Micro-structure and chemical composition of vateritic deformities occurring in the bivalve Corbicula fluminea (Müller, 1774). *J. Struct. Biol.* **174**, 321–332.

Fuge R. and Johnson C. C. (1986) The geochemistry of iodine—a review. *Environ. Geochem. Health* **8**, 31–54.

Gephart R. E. (2010) A short history of waste management at the Hanford site. *Phys. Chem. Earth* **35**, 298–306.

Please cite this article in press as: Feng X. and Redfern S. A. T. Iodate in calcite, aragonite and vaterite $CaCO_3$: Insights from first-principles calculations and implications for the I/Ca geochemical proxy. *Geochim. Cosmochim. Acta* (2018), https://doi.org/10.1016/j.gca.2018.02.017

Glock N., Liebetrau V. and Eisenhauer A. (2014) I/Ca ratios in benthic foraminifera from the Peruvian oxygen minimum zone: analytical methodology and evaluation as a proxy for redox conditions. *Biogeosciences* **11**, 7077–7095.

Glock N., Liebetrau V., Eisenhauer A. and Rocholl A. (2016) High resolution I/Ca ratios of benthic foraminifera from the Peruvian oxygen-minimum-zone: a SIMS derived assessment of a potential redox proxy. *Chem. Geol.* **447**, 40–53.

Graf D. L. (1961) Crystallographic tables for the rhombohedral carbonates. *Am. Mineral.* **46**, 1283–1316.

Hardisty D. S., Zhou X., Diamond C. W. and Lyons T. W. (2017) Perspectives on Proterozoic surface ocean redox from iodine contents in ancient and recent carbonate. *Earth Planet. Sci. Lett.* **463**, 159–170.

He L., Liu F., Hautier G., Oliveira M. J. T., Marques M. A. L., Vila F. D., Rehr J. J., Rignanese G. and Zhou A. (2014) Accuracy of generalized gradient approximation functionals for density-functional perturbation theory calculations. *Phys. Rev. B* **89**, 64305.

Hill R. (1952) The elastic behavior of a crystalline aggregate. *Proc. Phys. Soc. Lond.* **65A**, 349–354.

Jacob D. E., Wirth R., Agbaje O. B. A., Branson O. and Eggins S. M. (2017) Planktic foraminifera form their shells via metastable carbonate phases. *Nat. Commun.* **8**, 1265.

Kaplan D. I., Denham M. E., Zhang S., Yeager C., Xu C., Schwehr K. A., Li H. P., Ho Y. F., Wellman D. and Santschi P. H. (2014) Radioiodine biogeochemistry and prevalence in groundwater. *Crit. Rev. Environ. Sci. Technol.* **44**, 2287–2335.

Kaplan D. I., Roberts K. A., Schwehr K. A., Lilley M. S., Brinkmeyer R., Denham M. E., Diprete D., Li H. P., Powell B. A., Xu C., Yeager C. M., Zhang S. and Santschi P. H. (2011) Evaluation of a radioiodine plume increasing in concentration at the Savannah river site. *Environ. Sci. Technol.* **45**, 489–495.

Keeling R. F., Körtzinger A. and Gruber N. (2010) Ocean deoxygenation in a warming world. *Ann. Rev. Mar. Sci.* **2**, 199–229.

Kennedy H. A. and Elderfield H. (1987) Iodine diagenesis in non-pelagic deep-sea sediments. *Geochim. Cosmochim. Acta* **51**, 2505–2514.

Kontrec J., Kralj D., Brečević L., Falini G., Fermani S., Noethig-Laslo V. and Mirosavljević K. (2004) Incorporation of inorganic anions in calcite. *Eur. J. Inorg. Chem.*, 4579–4585.

Kresse G. and Furthmüller J. (1996) Efficient iterative schemes for *ab initio* total-energy calculations using a plane-wave basis set. *Phys. Rev. B* **54**, 11169–11186.

Lamble G. M., Lee J. F., Staudt W. J. and Reeder R. J. (1995) Structural studies of selenate incorporation into calcite crystals. *Phys. B Phys. Condens. Matter* **208–209**, 589–590.

Liu L. G., Chen C. C., Lin C. C. and Yang Y. J. (2005) Elasticity of single-crystal aragonite by Brillouin spectroscopy. *Phys. Chem. Miner.* **32**, 97–102.

Lu Z., Hoogakker B. A. A., Hillenbrand C. D., Zhou X., Thomas E., Gutchess K. M., Lu W., Jones L. and Rickaby R. E. M. (2016) Oxygen depletion recorded in upper waters of the glacial Southern Ocean. *Nat. Commun.* **7**, 11146.

Lu Z., Jenkyns H. C. and Rickaby R. E. M. (2010) Iodine to calcium ratios in marine carbonate as a paleo-redox proxy during oceanic anoxic events. *Geology* **38**, 1107–1110.

Maslen E. N., Streltsov V. A. and Streltsova N. R. (1993) X-ray study of the electron-density in calcite, $CaCO_3$. *Acta Crystallogr. Sect. B-Struct. Sci.* **49**, 636–641.

Nehrke G., Poigner H., Wilhelms-Dick D., Brey T. and Abele D. (2012) Coexistence of three calcium carbonate polymorphs in the shell of the Antarctic clam Laternula elliptica. *Geochem. Geophys. Geosyst.* **13**, Q05014.

Perdew J. P., Burke K. and Ernzerhof M. (1996) Generalized gradient approximation made simple. *Phys. Rev. Lett.* **77**, 3865–3868.

Perdew J. P., Chevary J. A., Vosko S. H., Jackson K. A., Pederson M. R., Singh D. J. and Fiolhais C. (1992) Applications of the generalized gradient approximation for exchange and correlation. *Phys. Rev. B* **46**, 6671–6687.

Peter S., Suchanek E., Roisnel T. and Lutz H. D. (1998) Neutron powder diffraction study on highly deuterated $Ca(IO_3)_2{\cdot}D_2O$. *Acta Crystallogr. Sect. C Cryst. Struct. Commun.* **54**, 1064–1066.

Podder J., Lin J., Sun W., Botis S. M., Tse J., Chen N., Hu Y., Li D., Seaman J. and Pan Y. (2017) Iodate in calcite and vaterite: Insights from synchrotron X-ray absorption spectroscopy and first-principles calculations. *Geochim. Cosmochim. Acta* **198**, 218–228.

Redfern S. A. T., Branson O. and Read E. (2017) Synchrotron X-ray microscopy of marine calcifiers: how plankton record past climate change. *J. Phys. Conf. Ser.* **849**, 12011.

Redfern S. A. T., Salje E. and Navrotsky A. (1989) High-temperature enthalpy at the orientational order-disorder transition in calcite: implications for the calcite/aragonite phase equilibrium. *Contrib. Mineral. Petrol.* **101**, 479–484.

Reeder R. J., Lamble G. M., Lee J.-F. and Staudt W. J. (1994) Mechanism of SeO_4^{2-} substitution in calcite: an XAFS study. *Geochim. Cosmochim. Acta* **58**, 5639–5646.

Rue E. L., Smith G. J., Cutter G. A. and Bruland K. W. (1997) The response of trace element redox couples to suboxic conditions in the water column. *Deep Res. Part I Oceanogr. Res. Pap.* **44**, 113–134.

Takano B., Asano Y. and Watanuki K. (1980) Characterization of sulfate ion in travertine. *Contrib. Mineral. Petrol.* **72**, 197–203.

Tzeng W. N., Chang C. W., Wang C. H., Shiao J. C., Iizuka Y., Yang Y. J., You C. F. and Ložys L. (2007) Misidentification of the migratory history of anguillid eels by Sr/Ca ratios of vaterite otoliths. *Mar. Ecol. Prog. Ser.* **348**, 285–295.

De Villiers J. P. R. (1971) Crystal structures of aragonite, strontianite, and witherite. *Am. Mineral.* **56**, 758–767.

Zhang S., Xu C., Creeley D., Ho Y. F., Li H. P., Grandbois R., Schwehr K. A., Kaplan D. I., Yeager C. M., Wellman D. and Santschi P. H. (2013) Iodine-129 and iodine-127 speciation in groundwater at the Hanford site, U.S.: Iodate incorporation into calcite. *Environ. Sci. Technol.* **47**, 9635–9642.

Zhou X., Jenkyns H. C., Owens J. D., Junium C. K., Zheng X. Y., Sageman B. B., Hardisty D. S., Lyons T. W., Ridgwell A. and Lu Z. (2015) Upper ocean oxygenation dynamics from I/Ca ratios during the Cenomanian-Turonian OAE 2. *Paleoceanography* **30**, 510–526.

Zhou X., Thomas E., Rickaby R. E. M., Winguth A. M. E. and Lu Z. (2014) I/Ca evidence for upper ocean deoxygenation during the PETM. *Paleoceanography* **29**, 964–975.

Associate editor: Thomas M. Marchitto

Please cite this article in press as: Feng X. and Redfern S. A. T. Iodate in calcite, aragonite and vaterite $CaCO_3$: Insights from first-principles calculations and implications for the I/Ca geochemical proxy. *Geochim. Cosmochim. Acta* (2018), https://doi.org/10.1016/j.gca.2018.02.017